Supporting information for: "Increased Photoconductivity Lifetime in GaAs Nanowires by Controlled n-Type and p-Type Doping"

Jessica L. Boland,[†] Alberto Casadei,[‡] Gözde Tütüncüoglu,[‡] Federico Matteini,[‡] Christopher L. Davies,[†] Fauzia Jabeen,[¶] Hannah. J. Joyce,[§] Laura M. Herz,[†] Anna Fontcuberta i Morral,[‡] and Michael B. Johnston*[,†]

†*Department of Physics, University of Oxford, Clarendon Laboratory, Parks Road, Oxford, OX1 3PU, United Kingdom*

‡*Laboratory of Semiconductor Materials, École Polytechnique Fédérale de Lausanne (EPFL), CH-1015 Lausanne, Switzerland*

¶*Laboratory of Quantum Optoelectronics, École Polytechnique Fédérale de Lausanne (EPFL), CH-1015 Lausanne, Switzerland*

§*University of Cambridge, Department of Engineering, 9 JJ Thomson Avenue, Cambridge CB3 0FA, United Kingdom*

E-mail: michael.johnston@physics.ox.ac.uk

Experimental Details

SEM Images

Figure S1 show tilted scanning electron micrographs of n-type (left) and p-type (right) nanowire homostructures. The images were taken prior to the transfer of the nanowires to quartz substrates.

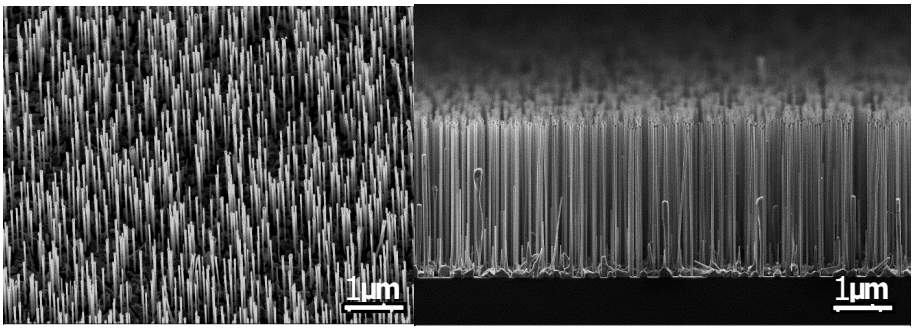

Figure S1: SEM images for nanowires as grown for both n-type (left) and p-type (right) samples.

Simulations of Photoexcited Carrier Density Profiles for the Doped Samples

NextNano simulations[S1] were carried out for both n-type and p-type GaAs nanowires under photoexcitation. A spatially uniform electron and hole distribution of $4 \times 10^{18}\,\mathrm{cm}^{-3}$ was added to the homostructure. Under photoexcitation, the band bending seen in equilibrium changes. The band bending flattens due to screening from photoexcited electrons and holes respectively. Figures S2a and b show the bandedge diagrams respectively for the n-type doped and p-type doped sample after initial photoexcitation. Due to the change in band bending, the electron and hole density profiles also change, as shown in Figure S2c and d. It can be seen that for the n-doped sample (Figure S2c), the electrons move to the surface and are kept away from the core. For the p-doped sample (Figure S2d), the holes

are mainly distributed within the shell, where recombination takes place and are also kept away from the core, contributing to the high hole mobility observed for this sample. The electron density is then confined to the surface, where trapping and recombination takes place, contributing to the fast initial carrier decay observed for this sample. Figure S2e and f show these electron and hole density profiles for these samples respectively. This coincides with the experimental results described within the main manuscript.

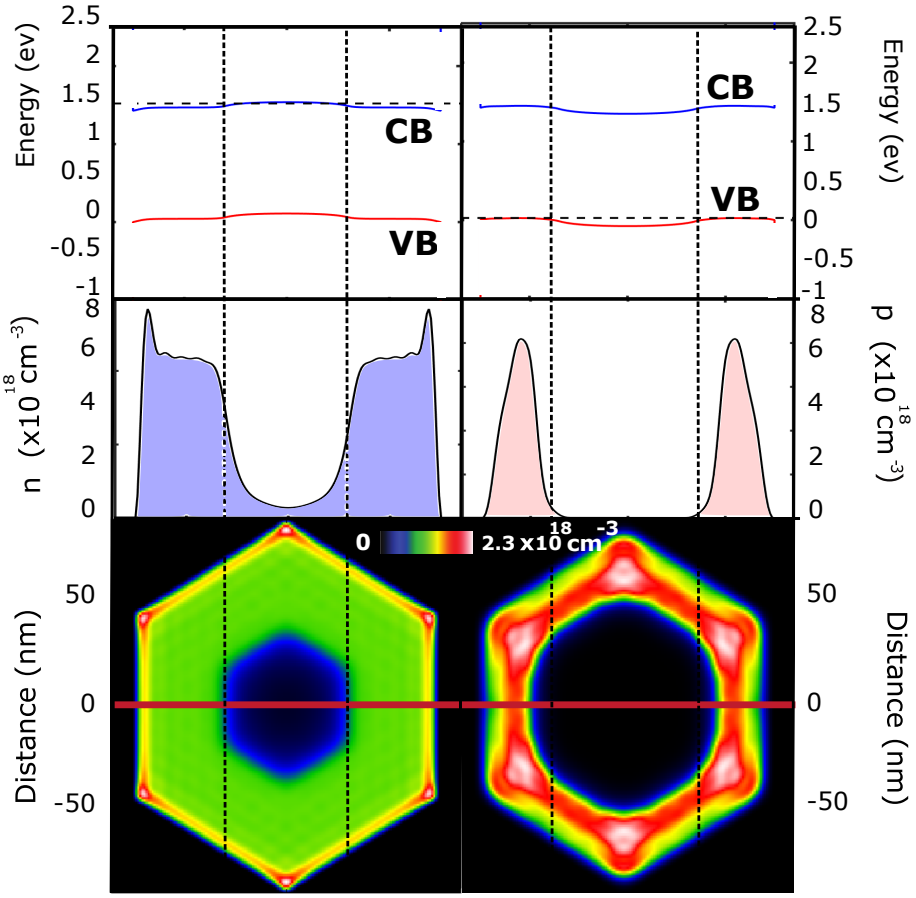

Figure S2: Nextnano simulations of n-doped (left) and p-doped (right) nanowires when photoexcited uniformly to a concentration of $n = p = 4 \times 10^{18}$ cm^{-3}. The first row plots the conduction band (CB) and valance band (VB) edges along a line through the centre of the nanowires, perpendicular to the long axis of the nanowire. The second row show the electron (hole) density along the same line. The bottom row is a colour map of the electron (hole) density of a cross-section through the nanowire perpendicular to its long axis.

Figure S3 shows simulations of the p-doped nanowires with an added initial uniform electron and hole distributions of $3 \times 10^{18}\,\mathrm{cm}^{-3}$, $1 \times 10^{18}\,\mathrm{cm}^{-3}$ and $8.5 \times 10^{17}\,\mathrm{cm}^{-3}$ were

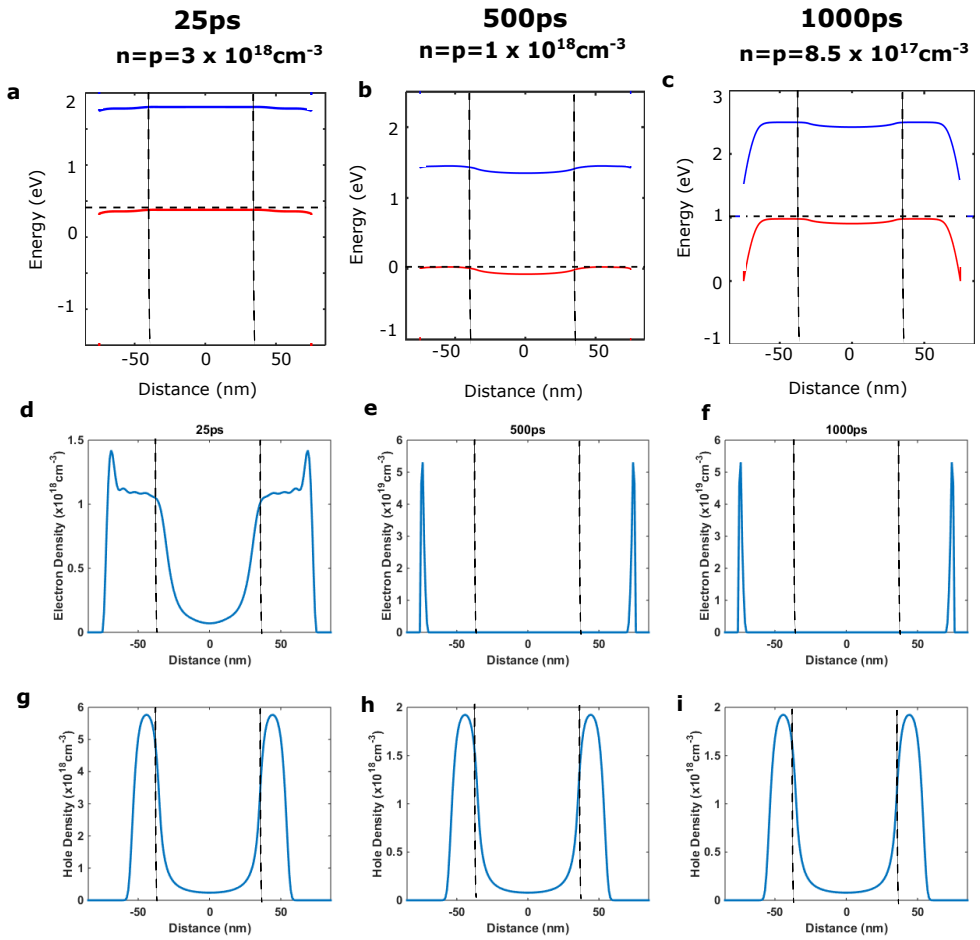

Figure S3: NextNano simulation of the band edge profile (a–c), and distribution of electrons (d–f) and holes (g–i) for a nanowire with a p-type shell ($35\,\mathrm{nm} < |x| < 75\,\mathrm{nm}$) and intrinsic core ($|x| < 35\,\mathrm{nm}$). Distance ($= x$) represents the radial distance from the central axis of the nanowire. The first column (a, d, g) show the results of the calculation for a photo-injected carrier concentration of $3 \times 10^{18}\,\mathrm{cm}^{-3}$, which corresponds to the carrier concentration at 25 ps after excitation in the terahertz photoconductivity experiments shown in Figure 4 of the main article. Likewise the second column (b, e, h) are the results of a calculation photo-injected carrier desnity of $1 \times 10^{18}\,\mathrm{cm}^{-3}$ corresponding to 500 ps after excitation and the third column (c,f,i) are for $8.5 \times 10^{17}\,\mathrm{cm}^{-3}$ corresponding to 1000 ps after photoexcitation.

added to the initial conditions of the simulation, and the simulations were then run until equilibrium charge distributions were achieved in the absence of any charge recombination. The three densities correspond roughly to the carrier densities at 25, 500 and 1000ps after photo-excitation for the experiments presented in Figure 4 of the manuscript. While the simulation does not take account of dynamics explicitly, this method provides a qualitative insight into the charge distributions as a function of time after photoexcitation as long as charge redistribution occurs on a much faster timescale than charge recombination.

Time Dependence of Photoconductivity Spectra for *n*-Type Doped Sample and Undoped Reference

Figure S4 presents photoconductivity spectra of n-doped, p-doped and undoped GaAs nanowires obtained at a range of different times after photoexcitation. The left–hand column shows displays spectra for the n-type doped sample, the middle column spectra for the p-type doped sample, while those in the right–hand column correspond to the undoped reference sample. Spectra were taken 25 ps, 100 ps, 250 ps and 1000 ps after photoexcitation with 1.55 eV ($\lambda = 800$ nm) at a fluences of 26 μJ cm^{-2}. All spectra for the n-type and undoped sample show a Lorentzian response, with the resonant frequencies (marked by the arrows in Figure S7) shifting to lower frequency with time after photoexcitation. The resonant frequency increasing with increasing carrier density is a key attribute of localised surface plasmon (LSP) modes. The resonant frequency is also clearly shifted to higher frequency for the bulk n-type doped sample (left column) compared with the undoped reference (right column) for each excitation fluence. This is related to the additional donated electrons in the doped nanowires, as described in the main manuscript. For the p-type doped sample, a Lorentzian response is seen at 25 ps after photoexcitation, yet beyond this time a Drude response with a short scattering time is observed. This is explained in the main manuscript and is attributed to the short mean free path of holes, causing them to no longer

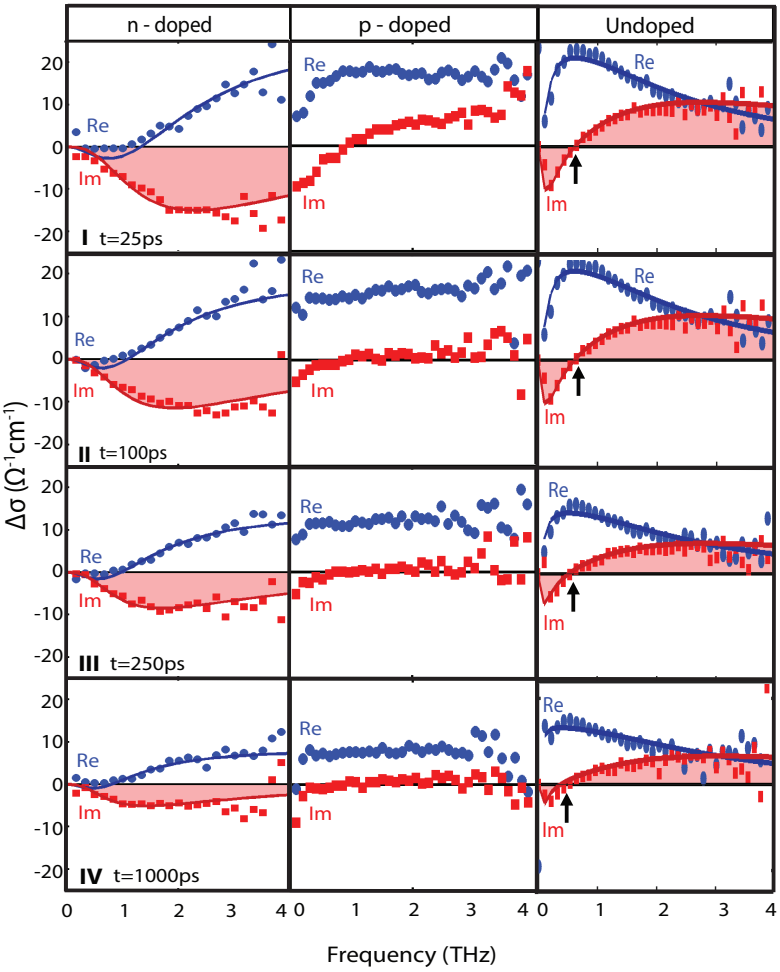

Figure S4: Time–resolved conductivity of photoexcited carriers for the n-doped, p-doped and undoped reference samples taken at times of 25 ps, 100 ps, 250 ps and 1000 ps after photoexcitation. The excitation photon energy, fluence and pulse duration were 1.55 eV, 25.5 μJ cm^{-2}and 35 fs respectively. All measurements were performed at room temperature.

feel localisation due to the nanowire dimensions.

Ensemble Photoluminescence Measurements

Time integrated photoluminescence (PL) measurements were performed on the ensembles of nanowires described in the the main text. The PL system has been described in detail previously.[S2] Figure S5 shows the photoluminescence measured from the p-doped nanowires (blue curve) and the undoped reference nanowires (red) curve. No PL could be observed from the undoped reference sample, as is usual for GaAs nanowires without surface passivation of capping layers at room temperature. In contrast the p-doped nanowires produced a strong PL signal. These results are consistent with a reduction in surface related SRH recombination (i.e. a reduction in k_1).

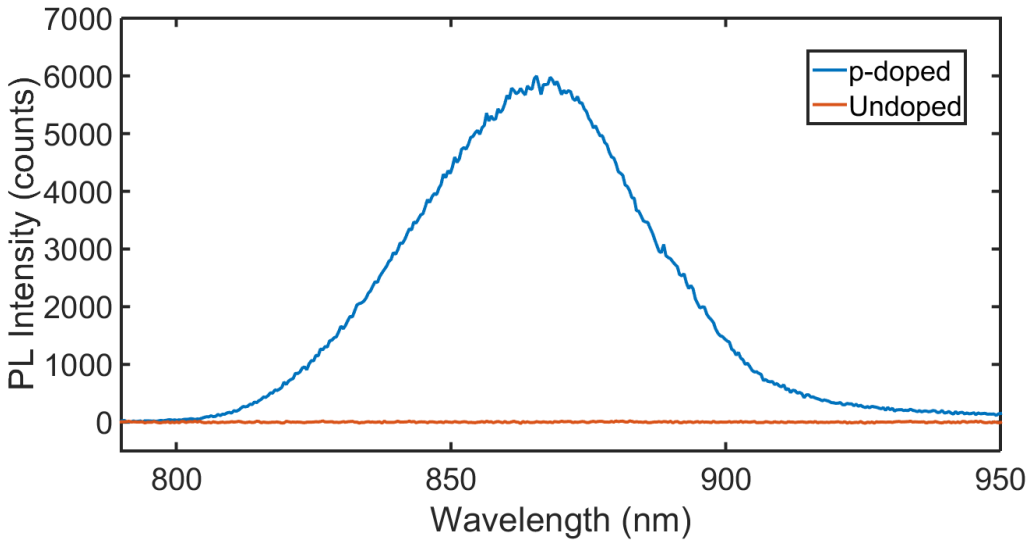

Figure S5: Time–integrated photoluminescence of an ensemble of nanowires with a p-doped shell (see main text for exact sample specifications) is shown by the blue curve. No PL signal could be obtained from the undoped reference sample under the same excitation and collection conditions. Measurements were performed at room temperature using the same sample on quartz substrates as were used for THz photoconductivity measurements. The spectra have been corrected for the spectral response of the PL system.

Data Analysis of THz Transmission Data

Conversion of THz Transmission to Photoconductivity

The photoconductivity, $\Delta\sigma$, is extracted from the OPTP measurements of $\frac{\Delta E}{E}$. The nanowires are considered to be embedded within a surrounding layer of thickness, d, which is the average diameter of the nanowire; and to have an effective areal fill factor obtained from optical microscope images.[S3] The transmitted terahertz fields with and without the optical pump are described as follows:

$$E_{\mathrm{on}} = f_{\mathrm{w}} E_{\mathrm{w}*} + (1 - f_{\mathrm{w}})\, E_{\mathrm{v}} \tag{1}$$

$$E_{\mathrm{off}} = f_{\mathrm{w}} E_{\mathrm{w}} + (1 - f_{\mathrm{w}})\, E_{\mathrm{v}}. \tag{2}$$

where E_{w} and E_{v} are the terahertz transmitted electric fields through the nanowires and surrounding vaccum respectively, with * denoting a photoexcited state. The pump beam does not change the complex refractive index of the vacuum, so the electric fields E_{v}, E_{w} and $E_{\mathrm{w}*}$ can be written as:

$$E_{\mathrm{v}} = e^{i n_{\mathrm{v}} \omega d/c} E_{\mathrm{i}} \tag{3}$$

$$E_{\mathrm{w}} = t_{\mathrm{vw}} t_{\mathrm{wv}} e^{i n_{\mathrm{w}} \omega d/c} F P_{\mathrm{vwv}} E_{\mathrm{i}} \tag{4}$$

$$E_{\mathrm{w}*} = t_{\mathrm{vw}*} t_{\mathrm{w}*\mathrm{v}} e^{i n_{\mathrm{w}*} \omega d/c} F P_{\mathrm{vw}*\mathrm{v}} E_{\mathrm{i}}. \tag{5}$$

where t_{ij} are the Fresnel transmission coefficients, FP_{ijk} the Fabry-Pérot terms, c is the speed of light and $n_{\mathrm{w}*}$, n_{w} the refractive indices for the nanowires with and without photoexcitation respectively. By combining Equations 1 and 2, the ratio of terahertz fields for the nanowires with and without photoexcitation is given in terms of the OPTP measurement

of $\frac{\Delta E}{E}$:

$$\frac{E_{w*}}{E_w} = \frac{\Delta E}{E}\left[1 + \left(\frac{1}{f_w} - 1\right)\frac{E_v}{E_w}\right] + 1. \tag{6}$$

where $\Delta E = E_{on} - E_{off}$, the photoinduced change in transmission and $E = E_{off}$, the THz transmission in the absence of photoexcitation. At THz frequencies, the thin film limit can be applied, as $\frac{n\omega\delta}{c} << 1$, so the approximation $\frac{E_v}{E_w} = 1$ can be made. By using this approximation, a parameter A can be defined:

$$A = \frac{E_w}{E_{w*}} = \frac{1}{\frac{1}{f_w}\frac{\Delta E}{E} + 1}. \tag{7}$$

By substituting in the appropriate FP_{ijk} and t_{ij} into Equation 3 and 4 and applying the thin film limit, the following equation is obtained:

$$\frac{E_{w*}}{E_w} = \frac{2 - \frac{i\omega d}{c}(1 + n_w^2)}{2 - \frac{i\omega\ d}{c}(1 + n_{w*}^2)}. \tag{8}$$

Substituting in the general relation $n^2 = \epsilon$ to the above equation:

$$\epsilon_{w*} = \left[-\frac{E_w}{E_{w*}}\left(2\frac{c}{i\omega d} - (1 + \epsilon_w)\right) + 2\frac{c}{i\omega d} - 1\right]. \tag{9}$$

where ϵ_{w*} and ϵw are the dielectric constants of the nanowires with and without photoexcitation respectively. The photoinduced conductivity, $\Delta\sigma$ is then given by:

$$\epsilon_{w*} = \epsilon_w + \frac{i\Delta\sigma}{\omega\epsilon_0}. \tag{10}$$

where ϵ_0 is the permittivity of free space. Substituting Equation 9 into Equation 10, the photoinduced conductivity can be extracted:

$$\Delta\sigma = \epsilon_0 (A-1) \left[\frac{2c}{d} - i\omega (1+\epsilon_w)\right]. \tag{11}$$

Thus, using Equations 7 and 11, the photoinduced conductivity can be extracted from OPTP measurements using $\epsilon_w = 12.95$ for bulk GaAs and values of f_w and d taken from optical electron microscope measurements.

Calculating the Photoexcited Carrier Density

The photoexcited carrier density, n_p for a sample of thickness d is given by:

$$n_p = \frac{I}{Ed}\left(1 - e^{-d/\alpha}\right). \tag{12}$$

where I is the photoexcitation fluence, E is the photon energy and α is the absorption depth at the excitation wavelength. The absorption depth, $\frac{1}{\alpha}$ for GaAs is approximately 1μm for photons with energy 1.55 eV ($\lambda = 800$ nm)[S4] . This absorption depth is significantly larger than the nanowire diameter studied, so the nanowires fall within the thin film limit. Therefore, for a given photoexcitation intensity, the photoexcited carrier density is approximately constant for the nanowire diameter.

Fitting Process for Carrier Decay Traces and Conductivity Spectra

The charge carrier recombination dynamics for nanowires depend on excitation fluence and are described by the following carrier rate equation:[S5]

$$\frac{dn\,(t)}{dt} = -k_1 n - k_2(n + n_0)n - k_3 n^3. \tag{13}$$

where k_1 is the decay constant describing the rate of mono-molecular processes, such as trap-assisted recombination, k_2 is the bimolecular recombination constant and k_3 is the rate for Auger recombination. This carrier rate equation was globally fitted to the experimental data, by fixing the decay constants for each different excitation fluence for each sample.

The fitting process is a nonlinear least-square fit that requires the following optimisation:

$$min_x ||f\,(x)\,||_2^2 = min_x \left(f_1\,(x)^2 + f_2\,(x)^2 + ...f_n\,(x)^2\right). \tag{14}$$

The fitting process starts from an initial point and minimises the sum of the squares of the function described above. A lower bound of zero was placed on all the fitting parameters to make sure that they remain positive and therefore physical.

The same fitting process was used to globally fit a Lorentzian conductivity response to the photoconductivity spectra with the doping density set as a global parameter for the undoped and doped sample respectively. The uncertainty for the doping density parameter calculated using the chi-squared non-linear regression was found to be 4.5 % for the undoped sample and 8.7 % and 9.4 % for the n-doped and p-doped samples respectively.

Calculation of Depletion Widths, Diffusion Lengths and Mean Free Path for Doped Samples

To further examine the effects of doping on the electronic and optical properties of GaAs nanowires, carrier transport across the core-shell interface must be considered. It can clearly be seen that bulk doping within the shell of the nanowire causes band bending at the interface and thus it is expected that there will be a diffusion and drift current across this interface. These currents will lead to a depletion region and built-in potential due to doping, allowing diffusion lengths and depletion widths to be determined, which can be used to provide explanations for the recombination mechanisms observed.

For both doped samples, the case of a one-side abrupt junction can be considered: n-i junction for n-type doping and p-i junction for p-type doping. At thermal equilibrium, the individual electron and hole currents flowing across the junctions are identically zero. Thus, the drift current due to the electric field induced must directly cancel with the diffusion current due to the concentration gradient. This leads to the Fermi level remaining constant throughout the nanowire, creating a unique space charge distribution across the interface. This space charge distribution and electrostatic potential, ψ , are given by the Poissons equation:

$$\frac{d^2\psi}{dx^2} = -\frac{d\xi}{dx} = \frac{-q}{\epsilon}\left(N_D - N_A + p - n\right) \tag{15}$$

where ϵ is the permittivity of the nanowire, N_D is the donor density, N_A is the acceptor density, p is the hole concentration and n is the electron concentration. Here, we assume that all donors and acceptors are ionised. By expressing the hole concentration as $p = n_i e^{\left(E_i - E_f\right)/k_b T}$ and the electron concentration as $n = n_i e^{\left(E_f - E_i\right)/k_b T}$ and assuming that for the p-doped region, $N_D = 0$ and the n-doped region, $N_A = 0$, the total electrostatic potential

is determined to be:

$$V_{\mathrm{bi}} = \psi_n - \psi_p = \frac{k_b T}{q} ln\left(\frac{N_A N_D}{n_i^2}\right) \tag{16}$$

This is called the built-in potential and is defined as the electrostatic potential within the depletion region. Thus, it can also be expressed as:

$$\begin{aligned} V_{\mathrm{bi}} &= \int_{-x_p}^{x_n} \xi\left(x\right) dx = -\int_{-x_p}^{0} \xi\left(x\right) dx - \int_{0}^{x_n} \xi\left(x\right) dx \\ &= \frac{qN_A x_p^2}{2\epsilon} + \frac{qN_D x_n^2}{2\epsilon} \end{aligned} \tag{17}$$

where x_p is the distance from the centre of the junction to the end of the depletion region for the p-type region and x_n is the distance from the centre of the junction to the end of the depletion region for the n-type region. Thus the depletion width, W, is given by: $W = x_p + x_n$. From the above equation, the depletion width is calculated to be:

$$W = \sqrt{\frac{2\epsilon}{q}\left(\frac{N_A + N_D}{N_A N_D}\right) V_{\mathrm{bi}}} \tag{18}$$

For the the nanowires described in the manuscript, $\epsilon = 12.95\epsilon_0$ and $n_i = 2.25 \times 10^6 \mathrm{cm}^{-3}$. For the p-doped sample, $N_A = 1.38 \times 10^{18} \mathrm{cm}^{-3}$ and $N_D = n_i$; and for the n-doped sample, $N_D = 1.38 \times 10^{18} \mathrm{cm}^{-3}$ and $N_A = n_i$. This gives a depletion width of 5.94 nm for both doped samples.

The diffusion rates for holes and electrons were calculated using mobilities extracted from experimental data inputed into the following equation:

$$D = \frac{k_b T \mu}{q} \tag{19}$$

The diffusion lengths, $L = (D\tau)^{1/2}$, could then be calculated for both doped samples and compared to the depletion widths. It was found that the diffusion length for the holes in the p-doped sample was shorter than for the electron diffusion length in the n-doped sample, showing that less migration of holes into the core with p-doping, leading to greater recombination in the nanowire shell.

The mean free paths for electrons and holes were calculated using: $\gamma = v\tau$, where the velocity for electrons in GaAs was found to be $4.65 \times 10^5 \mathrm{ms}^{-1}$ and for holes to be $1.63 \times 10^5 \mathrm{ms}^{-1}$. The scattering times for holes and electrons were taken from the experimental data.

References

(S1) Birner, S.; Zibold, T.; Andlauer, T.; Kubis, T.; Sabathil, M.; Trellakis, A.; Vogl, P. Nextnano: General Purpose 3-D Simulations. *IEEE Trans. Electron Devices* **2007**, *54*, 2137–2142.

(S2) Parkinson, P.; Knappke, C. E. I.; Kamonsutthipaijit, N.; Sirithip, K.; Matichak, J. D.; Anderson, H. L.; Herz, L. M. Ultrafast Energy Transfer in Biomimetic Multistrand Nanorings. *J. Am. Chem. Soc.* **2014**, *136*, 8217–8220.

(S3) Joyce, H. J.; Wong-Leung, J.; Yong, C.; Docherty, C. J.; Paiman, S.; Gao, Q.; Tan, H. H.; Jagadish, C.; Lloyd-Hughes, J.; Herz, L. M.; Johnston, M. B. Ultra-Low Surface Recombination Velocity in InP Nanowires Probed by Terahertz Spectroscopy. *Nano Lett.* **2012**, *12*, 5325–5330.

(S4) Casey, H. C.; Sell, D. D.; Wecht, K. W. Concentration-Dependence of Absorption-

Coefficient for n-Type and p-Type GaAs between 1.3 and 1.6 eV. *J. Appl. Phys.* **1975**, *46*, 250–257.

(S5) Aspnes, D. E. Recombination at Semiconductor Surfaces and Interfaces. *Surf. Sci.* **1983**, *132*, 406–421.